High performance liquid-solid tubular triboelectric nanogenerator for scavenging water wave energy

Qianxi Zhang [a,b], Ming He [a,b], Xinxiang Pan [a,b], Dandan Huang [a,b], Huahui Long [a,b], Mingsheng Jia [a,b], Zhiqiang Zhao [a,b], Cheng Zhang [a,b], Minyi Xu [c,*], Shishi Li [a,b,**]

[a] School of Mechanical and Power Engineering, Guangdong Ocean University, Zhanjiang 524088, China
[b] Technical Research Center for Ship Intelligence and Safety Engineering of Guangdong Province, Guangdong Ocean University, Zhanjiang 524088, China
[c] Marine Engineering College, Dalian Maritime University, Dalian 116026, China

ABSTRACT

The exploitation of clean and renewable wave energy has attracted fully concern in the world wide. In this work, a high-output array of liquid-solid tubular triboelectric nanogenerator (LST-TENG) based on the contact electrification between PTFE and water was proposed. The low-frequency wave motion was simulated to systematically analyze the impacts of several factors on the electrical performance of LST-TENG to provide guidance for the fabrication of the PTFE tube and the electrode arrangement for the achievement of high wave energy transition. An increase in the length/diameter of the tube, distance and width of the electrodes made a positive impact on the output performance of LST-TENG unit. A typical LST-TENG here should be an optimum water-to-cylinder volume ratio, as well it is better to wrap electrodes from the end, especially for short electrodes. Moreover, the influences of the motion characteristics including the angle, frequency and amplitude of oscillation was also considered. To achieve high peak output, we compared the output performance of series-wound and parallel LST-TENG arrays to find that parallel connection showed linear rise with the number of units is a feasible approach to get peak output voltage exceed 500 V, which extended the potential application of the LST-TENG arrays. At the optimal operating condition, the power density achieved 228 mW/m^3. This study provided the assessment of the power quality of LST-TENG and considering the diverse motion of the TENG units integrated into the blocks, which is expected to be the reference for the optimization of LST-TENG in the future.

1. Introduction

The growing crisis of energy shortage and environmental pollution has become a global issue, and the utilization of clean and renewable energy attracts focus around the world[1–3]. The ocean accounts for over 70% of the earth's surface, providing a great amount of wave energy. Wave energy has the advantages of easy exploitation, high energy flux density, wide distribution and weak environmental impacts[4,5], which has been exploited for a few decades and achieved commercial application[6,7]. The most common form of marine wave energy converters is the electromagnetic generator (EMG) based on Faraday law of electromagnetic induction, which was generally applied to large-capacity power units [8,9]. However, it is costly to construct power grids, maintain the power units and store electrical energy in long-distance offshore power plants. In recent years, Electrostatic-based

triboelectric nanogenerators (TENGs) with a variety of structures were developed to harvest disorder energy in the living environment such as human motions[10,11], mechanical vibration[12], wind[13] and wave energy[14–16]. TENG has been proved to be a promising energy convertor to harvest wave energy with the advantages of high energy density, low weight and low price[17–20]. TENG based on rolling electrification was demonstrated to be a feasible approach to harvest mechanical energy with up to 55% efficiency [21]. The output performance was improved by designing a hierarchically spherical TENG [22], as well as using silicone rubber balls[23] and silicone rubber balls with inner liquid[24] as the dielectric layer to enhance the contact area.

Until now, most of the reported TENGs were designed on the basis of the solid-solid friction effect, which requires an extremely dry environment to ensure high output. Moreover, the friction of solid-phase materials also shortens the lifetime. To overcome these shortcomings,

researchers turned their focus to liquid-solid interfacing TENGs that use liquid as one of the frictional layers, which contributes to full contact with the other solid layer. Benefiting from little shape-restriction of the liquid material, fluid-solid TENG shows outstanding performance in harvesting disorder energy. Fluid-solid TENGs utilized in collecting different forms of water energy such as droplets[25,26], running flow [27] and ocean waves[28,29] were reported. The electrical performance of liquid-solid tubular TENG was also widely used as sensors according to the liquid-solid contact-electrification mechanism. Wang et al.[30] designed the sensing part of the flow sensor in the form of a U-tube structure, the differential pressure in the Venturi tube generated liquid solution flows downward and upward along the left and right column respectively, resulting in electric potential difference. Zhang et al. [31] reported a water-based TENG as a sensor for the detection of organics in water by using a commercial PTFE filtration membrane. As a sensor, it requires modest output characteristics. Nevertheless, it is crucial to improve the electric output by means of effective energy conversion to expand the application of the water-based TENG. Then they prepared a new organic coating TENG based on fluorine-modified acrylate resin to enhance the contact electrification[32]. Later an array combination of water-based TENG was fabricated to collect the wave energy for all-weather cathodic protection[33]. To raise the peak power and signal-to-noise ratio, the working mechanism of the instantaneous discharging of Water-Tube-Based TENG was investigated [34]. Park et al. [27]designed a TENG based on the contact electrification between a PTFE nanowire coated Ti-mesh and water flow to get a high short-circuit current. It was demonstrated that several methods contribute to raising the energy-harvest efficiency. Beyond that, the effects of diverse factors on surface contact electrification have been investigated, the results demonstrated that these interrelated factors regulate solid-liquid triboelectricity in a synergistic or antagonistic manner[35]. Furthermore, as long as the TENG units work in synergy, the integration of TENG units as a power supply is another way to achieve a powerful output. Wu et al. [36] applied the integrated water-tube TENGs with high performance and simple fabrication to harvest body motion and ocean wave motion to explore the possibility of utilizing the WT-TENG for scavenging low-frequency motion energy. Although these studies discovered multiple marine applications of TENGs with varied structure for scavenging wave energy, it still lacks a detailed evaluation of the power quality, which is important for the power management and load match.

In this work, we aimed at evaluating the electrical output quality of LST-TENG and exploring the optimal approaches to integrated the LST-TENGs for the low-frequency wave energy harvest. The low-frequency wave motion was simulated to systematically analyze the impacts of several factors on the electrical performance of LST-TENG units to provide guidance for the shape of the PTFE tube and the electrode arrangement. Short-circuit current, open-circuit voltage and transferred charges were obtained to characterize power outputs. The electrical output was analyzed based on alternating current power supply, which is the formal state of the LST-TENG in the ocean. The influence of the connection mode of the TENG units has been study but the arrangement mode in the TENG blocks needs to be investigated to achieve large-scale integration. LST-TENGs arranged in the box at different positions were involved in the swing motion at diverse angles and amplitudes, whose effects on the output performance were investigated to provide guidance for the fabrication of the integrated LST-TENG boxes. Swing motion in low frequency with various amplitudes and oscillation angles was employed to simulate the power supply of the LST-TENG units assembled in different layers in the LST-TENG blocks floating in sea waves. The durability test was also performed to assess the offshore working possibility without manual maintenance. Moreover, strategies proposed based on the experimental results were applied to the arrangement of LST-TENG arrays, which were developed for harvesting wave energy with high efficiency for self-powered offshore devices.

2. Experimental sections

2.1. Structure of LST-TENG

The design and fabrication process of the LST-TENG is schematically illustrated in Fig. 1. As can be seen in Fig. 1(a), the LST-TENG network was assumed to be a large-scale power plant over the ocean. The integrated LST-TENG arrays composed of several units were sealed by an insulation and waterproof framework as a block to harvest water wave energy (as shown in Fig. 1(b)). Poly tetra fluoroethylene (PTFE) is one of the ideal materials to be the frictional layers of TENG since it has excellent hydrophobic surface and electron accepting capacity, satisfying chemical stability and aging resistance. PTFE tubes with a length of 10–30 cm, an inner diameter of 18 mm and a thickness of 1 mm were utilized to be one of the triboelectric layers. The structure of a LST-TENG unit was shown in Fig. 1(c), deionized (DI) water was encapsulated in a particular tube in PTFE with plugs in both two sides and copper film wrapped on two sides to work as electrodes. Furthermore, the special nano-fiber structure could increase the effective friction area of the material surface. Fig. 1(d) displayed the microscopic topography of the PTFE surface which has satisfied roughness for the effective friction to get electrified.

2.2. Methods

Ocean wave can be assumed as a sinusoidal motion in the study of water wave harvest[8,37,38]. To simulate the float motion of the LST-TENG units over ocean waves, an electromotor with variant deflection angles was used to drive the TENG units fixed on the extended arm to swing at a regular frequency and amplitude. A schematic diagram of the experimental apparatus was shown in Fig. 2(a), TSL-TENG units oscillated between the position L and R (L and R denote the largest intersection angle with the original position O on both sides, respectively). The electrical output included open-circuit voltage, short-circuit current and transferred charges were measured by an electrometer (Keithley 6514) coupled with a data acquisition module (National Instruments, DAQ-9174). The data acquisition frequency was set as 500 Hz. In this experiment, the influence of the frequency (F = 0.1–0.5 Hz), amplitude (35–95 cm) and oscillation angle ($30°$, $60°$, $90°$) of the motion were investigated. Moreover, electrical performance of different structure of the units were estimated by changing the length-to-diameter (L/D) ratio (5−15), injected water-to-cylinder volume ratios (WVR = 30%−70%), width (W = 6−14 cm) and the distance (D = 0.5–2.5 cm) of electrodes.

Furthermore, output power and internal resistance are also significant for power supplies, The internal resistance of the LST-TENG was measured following two methods. Schematic diagram of the circuit for the test was shown in Fig. S1 of the supplementary material.

Method 1: In Fig. S1, LST-TENG was equivalent to an ideal capacitor and a resistor. K denotes switch, R_I and R_L denote internal resistance and external load resistance respectively. The internal resistance of LST-TENG can be measured by obtaining the voltage of two different external load resistance (denote as U_L in Fig. S1), which follow Eqs. (1) and (2).

$$U_{\text{LST-TENG}} = U_1 + \frac{U_1}{R_{L1}} \quad R_I \tag{1}$$

$$U_{\text{LST-TENG}} = U_2 + \frac{U_2}{R_{L2}} \quad R_I \tag{2}$$

Where $U_{LST-TENG}$ denotes the output voltage of LST-TENG, R_{L1} and R_{L2} denotes the two different external load resistance connected in series respectively, U_1 and U_2 denotes the output voltage of R_{L1} and R_{L2} respectively. R_I can be derived from the combination of Eqs. (1) and (2), which can be put into Eq. (1) to get $U_{LST-TENG}$.
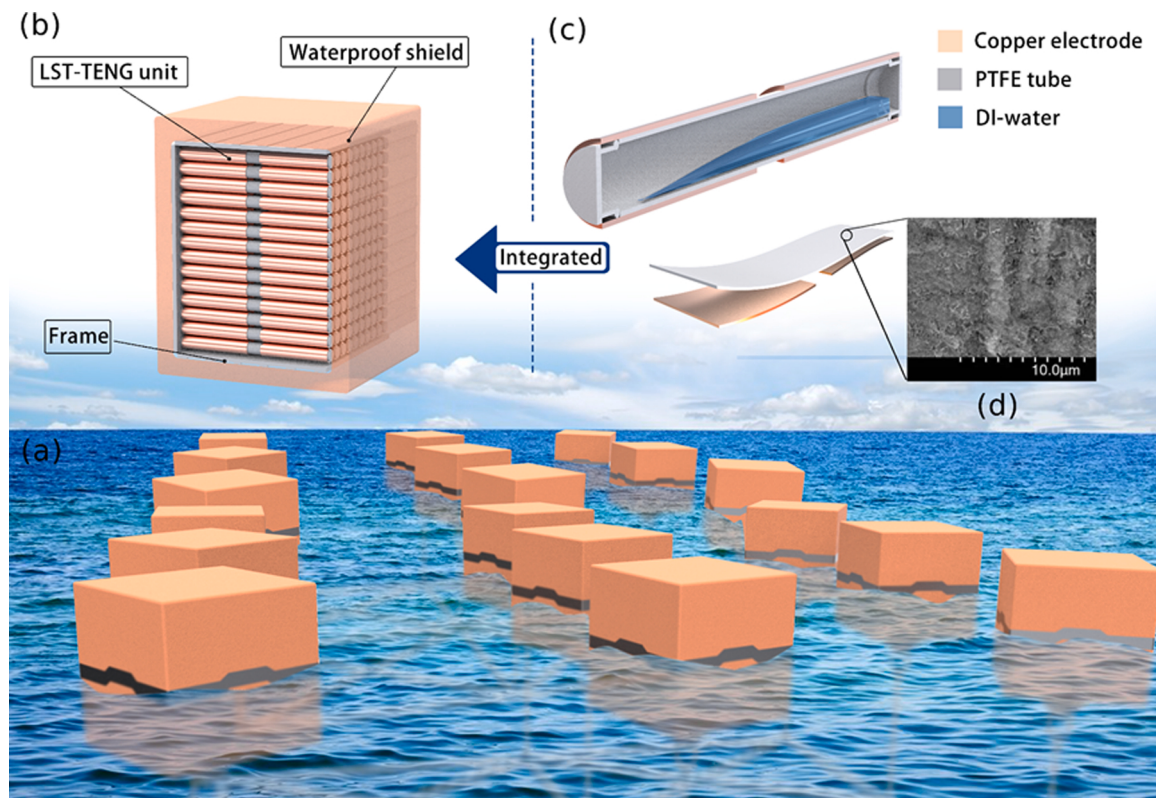
Fig. 1. The design and fabrication of the LST-TENG network. (a) LST-TENG network floating on the ocean, (b) fabrication of the LST-TENG blocks, (c) structure of a LST-TENG unit, (d) microscopic topography of PTFE surface.
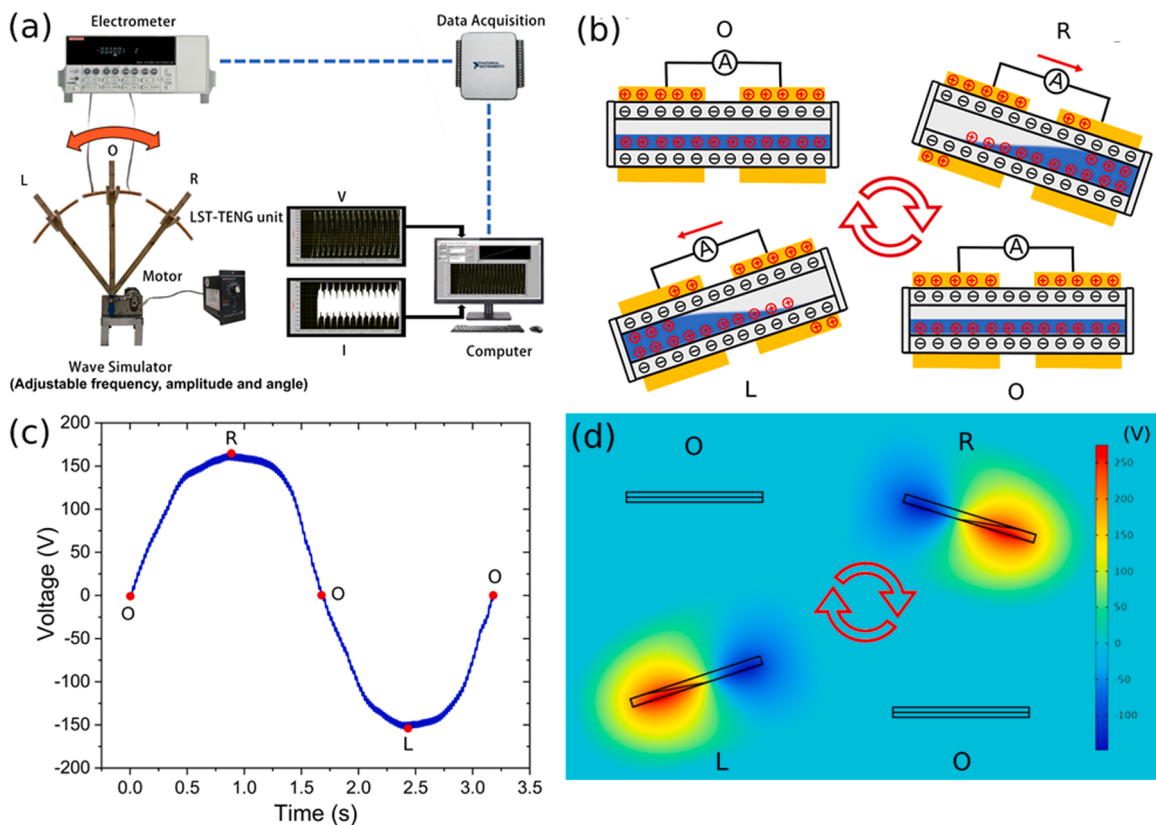

Fig. 2. Working mechanism of the LST-TENG. (a) Schematic diagram of the experimental apparatus, (b) liquid and charge distribution at characteristic states, (c) electrical output of a LST-TENG unit in a typical motor period, (d) calculated potential distribution at characteristic states.

$$R_I = \frac{2(U_1 - U_2)}{U_2 - 2U_1} R_{L1} \tag{3}$$

Method 2: To investigated the maximum output power of LST-TENGs, the fixed resistor in Fig. S1 was replaced by a variable resistance box with high precision. The voltage of the variable resistances (R_L) were measured by the electrometer. By this means, the output power of LST-TENG ($P_{LST-TENG}$) can derived by Eq. (4).

$$P_{LST-TENG} = R_L \left(\frac{U_{LST-TENG}}{(R_1 + R_L)} \right) \tag{4}$$

Where $U_{LST-TENG}$ denotes the output voltage of LST-TENG. Taking the derivative of Eq. (4) gets Eq. (5).

$$P'_{LST-TENG} = U^2_{LST-TENG} \frac{(R_I + R_L)(R_I - R_L)}{(R_I + R_L)^4} \tag{5}$$

Eq. (5) demonstrated that it gets maximum output power when the load resistance was equal to the internal resistance of the power supply. At this condition, the maximum output power can be determined by Eq. (6).

$$P_{\max} = \frac{U^2_{LST-TENG}}{4R_I} \tag{6}$$

In this work, the maximum peak output power was obtained, and the internal resistance of the LST-TENG equals to the external load resistance corresponding to the highest power. The internal resistance measured by these two methods were consistent.

3. Results and discussion

3.1. Working principle of the LST-TENG unit

The working mechanism of LST-TENG was depicted in Fig. 2(b). The working principle of the LST-TENG unit relies on the contact electrification effect, which makes electrons move from DI water into the PTFE surface, resulting in the negatively charged PTFE and positively charged DI water. Consequently, the formation of an electric double layer at the liquid-solid interface derives an electric potential difference between two electrodes[39,40]. Fig. 2(c) shows the open-circuit voltage of a LST-TENG unit in one motor period. At the horizontal position (position O in Fig. 2(a) and Fig. 2(b)), DI water evenly distributed along the PTFE tube, it shows little potential difference between the electrodes. When the LST-TENG unit moves side by side (position L and R in Fig. 2(a) and Fig. 2(b)), the DI water carrying positive charges moves to one side, which breaks the electrical balance and drives electrons to rearrange in the electrodes to achieve a new electrostatic balance. In the meanwhile, electrons transfer in the external circuit to balance the polarizing charge distribution caused by liquid motion.

When the DI water contacts the surface of the tubes, negative charges tend to transfer from water to PTFE through the interfaces due to the contact electrification effect, which leads to positively charged DI water and negatively charged PTFE tubes. DI water carrying charges flowing in the tube makes the charges at the interfaces rearranged to return electrostatic balance. Two copper tapes wrapped at the sides of tubes were utilized as electrodes and the bias of the electrostatic balance leads to potential difference at the two electrodes. It can be seen in Fig. 2(c), the largest potential difference (L and R) occurred at the extreme positions on the left and right, which corresponding to the potential distribution calculated by COMSOL Multiphysics based on finite element analysis in Fig. 2(d).

3.2. Influence of the LST-TENG structure on the electrical performance of the units

Current depicts the amounts of transferred charges through the

section for a period, thus they show the same tendency in this work. The correlations between the peak output performance and the structural parameters were investigated at the oscillation motion with a frequency of 1/3 Hz, an angle of 60°, an amplitude of 65 cm. Except for the peak output, the electrical output waveform was also diverse for different structure, the output voltage and current wave of the LST-TENG unit were illustrated in the supplementary material (Fig. S2). Moreover, the output power of the LST-TENG units under variant load resistance was shown in Fig. S3 of the supplementary material.

Fig. 3(a) shows the dependency of the output peak short-circuit current, open-circuit voltage, transferred charges and the maximum peak output power with the length-to-diameter (L/D) ratio of the LST-TENG units with 50% water volume (WVR) and 80% wrapped electrode area. It can be seen that the output peak voltage, current and maximum output power showed increased tendency that agreed well with the rise of L/D. Since the units with higher L/D accumulated more charges on the surface, which results in a higher potential difference between the two electrodes. As shown in Fig. 3(b), the electrical output of the units with variant injected water-to-cylinder volume ratios increased at the conditions of less than 47.5% and then declined. The filled-in volume for the highest output was closed to the coverage area of the electrodes (around 46.7% for the electrode with a 14 cm width), which demonstrated that when all water collects at one side leads to the largest potential difference. In order to further study the effect of electrode width, different wrapped ways were compared in Fig. 3(c), m-e denotes from middle to the end, e-m denotes from the end to middle. For both ways, the output voltage and current increased with the width of the electrodes and go to the same at 14 cm, while it showed higher for the units wrapped from the end for shorter electrodes. It indicated the reduced width has a more significant impact on the way that the electrodes wrapped from the middle.

Moreover, the effect of the distance for the electrodes with a width of 2×12 cm was also investigated. The result was illustrated in Fig. 3(d), the electrical output show a bit increase with the distance, which further proves that it is beneficial to wrap the electrodes from the end to get higher peak output. As the distributed density of the charges is higher at the terminals rather than the middle of the units (as shown in Fig. 2(d)). By comparing Fig. S2(d) and (e), it is found that the output wave for the m-e method is flatter than that of the e-m method, accordingly the peak/average ratio of the voltage is lower (as shown in Fig. 3(e)). The peak/average ratio of the voltage is the product of the form factor and crest factor, which were important parameter to evaluate whether the power supply meets the requirements of the electrical load. For the same electrode width, the output power for the electrodes wrapped from middle was lower than that of the electrodes wrapped from the end, and the peak/average output for the former also lower. In this work, LST-TENGs with shorter electrodes have lower maximum output power (as shown in Fig. 3(c)) but higher peak/average power. Some electronics require power adapters to have a large peak output/average output power ratio, which can provide peak power to the responsible device for a short period of time while significantly reducing the output power of the non-operating device. Evaluating the peak/average output helps to design the LST-TENG to meet various electrical requirements by structural changes.

3.3. Influences of the motion characteristics on the energy harvesting of LST-TENG units

To study the effects of the motion characteristics on the energy harvesting, the electrical output of LST-TENG units with a L/D ratio of 15, a filled water volume of 50% and an electrode width of 2×14 cm driven by oscillation motions with different angles, amplitudes and frequencies were obtained. From the schematic diagram of the distributed water and charges in Fig. 2(b), it is obvious that the difference in the contact area of water and PTFE surface increased with the oscillation angle and reached the maximum at 90°. For this reason, it is shown in
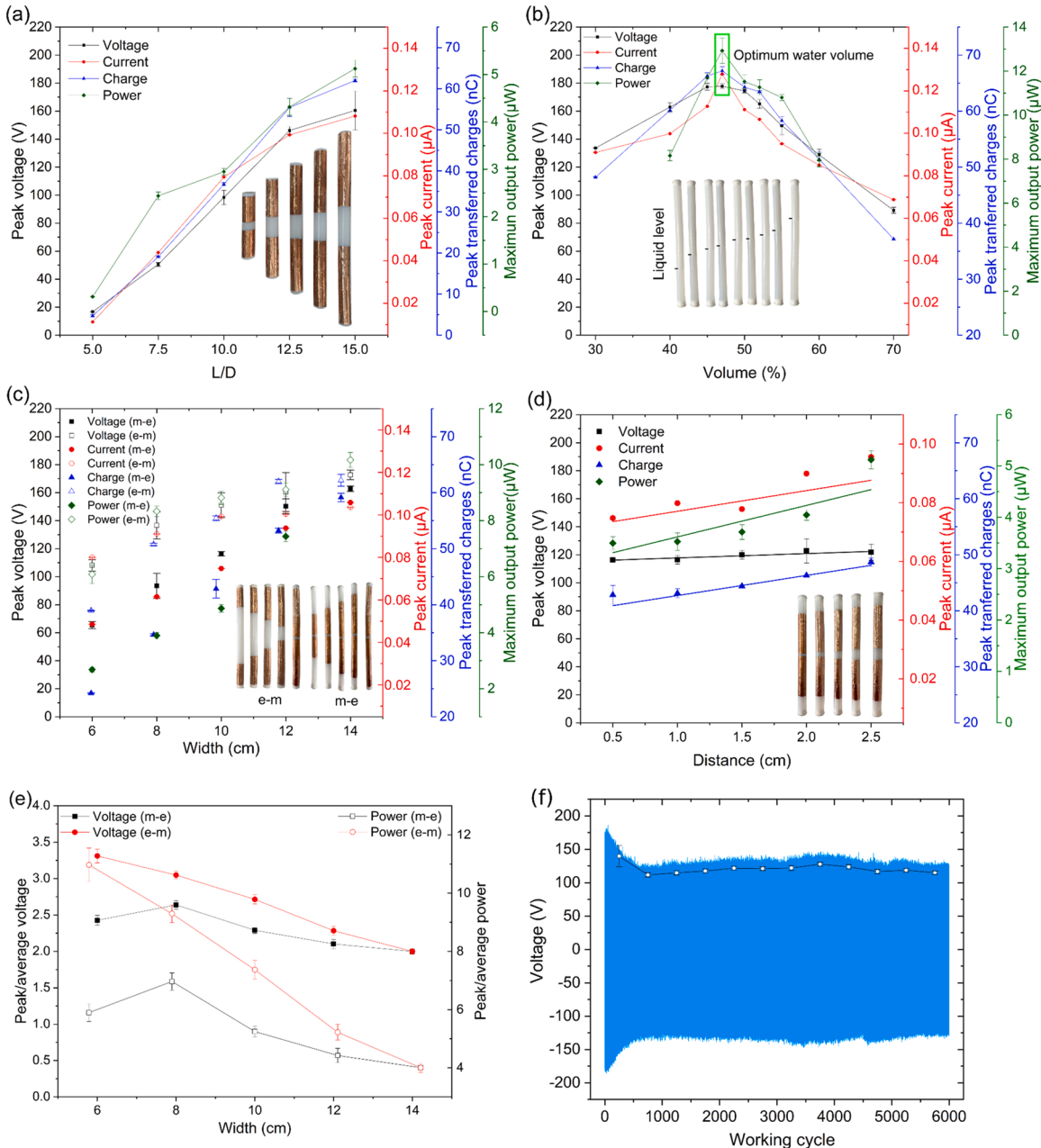
Fig. 3. Electrical output of LST-TENG units in different structures. (a) PTFE tubes with variant L/D (WVR = 50%, W = L/2.5), (b) DI water filled in variant volume (L = 30 cm, W = 2 ×14 cm), (c) variant width of the electrodes wrapped in different ways, m-e denotes from middle to the end, e-m denotes from the end to middle (WVR = 50%, L=30 cm), (d) variant distance of the electrodes (WVR = 50%, L = 30 cm, W=2 ×12 cm), (e) peak/average ratio of the voltage at variant electrode width, (f) durability of LST-TENG units.

Fig. 4(a) that the oscillation angle has a significant influence on the output of LST-TENG units, a larger angle contributes to higher peak output. The effect of the oscillation amplitude is similar to that of oscillation angle (shown in Fig. 4(b)), but it attributes to the higher flow rate in the PTFE tube at the condition of higher linear velocity. Besides, the frequency of the oscillation motion has a greater influence on the output of LST-TENG units. It is shown in Fig. 4(c) that the output cycles of the voltage and current matches the motion cycles well and the peak output increased with the frequency. The impact on the waveform was shown in Fig. 4(d), which indicated that the motion with a lower frequency and wider angle is favorable to achieving lower peak/average ratio. Furthermore, the durability of the LST-TENG unit was investigated and the results were displayed in Fig. 3(f). It can be seen that the output peak voltage showed a 20% decrease during the first 750 working cycles

and tended to be stable for a long time, which demonstrated that it is great advantage to fabricate maintenance-free LST-TENG by utilizing liquid-solid friction layers that caused minimal abrasion.

3.4. Arrangement and fabrication of TENG arrays

From the discussion above, it is feasible to enlarge the L/D ratio to get higher output but it causes other problems such as disorder deformation. To demand the request of the practical device, the LST-TENG units have to be integrated as arrays to get satisfying electrical output. The most common ways for the integration of power supply are series-wound and parallel arrangement. In general, the serial operation is a typical way to achieve high-output power supply, while parallel operation enhances reliability and enlarges the capacity of the power supply.
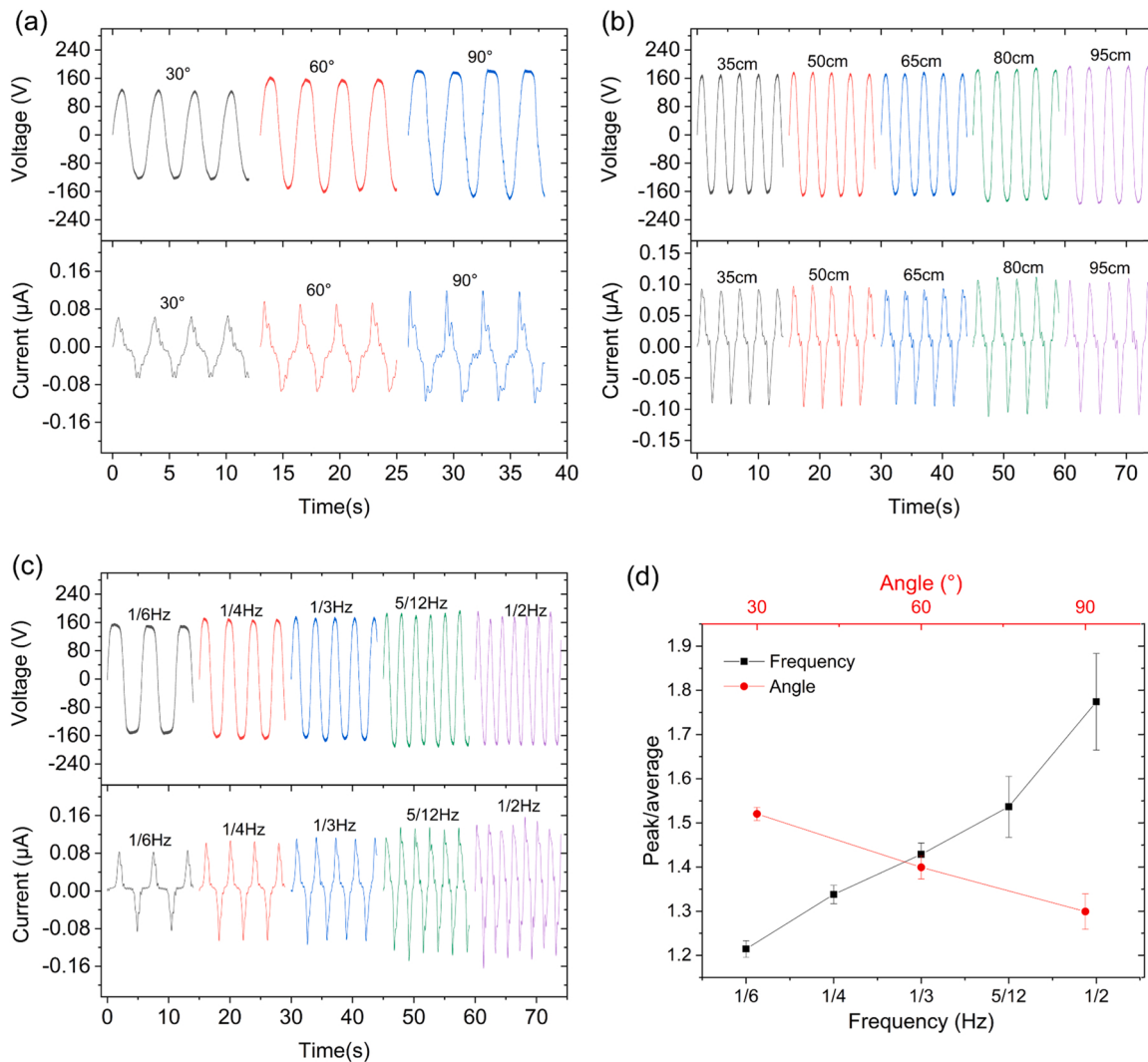
Fig. 4. Output voltage and current from diverse oscillation motion. (a)Variant limited angle with a frequency of 1/3 Hz and an amplitude of 65 cm, (b) variant amplitude with a frequency of 1/3 Hz and an angle of 60°, (c) variant frequency with an amplitude of 65 cm and an angle of 60°, (d) peak/average ratio of the voltage for oscillation motions with variant limited angle and frequency.

The connection mode among the units of the arrays affects the electrical output performance of the LST-TENG block. Conventionally, it is effective to improve the output voltage and current by connecting power units in the series method and parallel method respectively. To verify if this theory works for LST-TENG, amounts of composed units ranging from 2 to 10 were packaged in serial and parallel mode to investigate the synthetic effect.

The series connection mode was displayed in Fig. 5(a), the positive and negative electrodes of the LST-TENG units were connected end to end by conductive tapes. Differently, parallel arrays were obtained by connecting the same terminals of electrodes for each LST-TENG unit, which was depicted in the photograph and schematic diagram in Fig. 5 (b). The series-wound way is applied to the LST-TENG arrays firstly and the outputs of the arrays with different unit amounts are shown in Fig. 5 (c), which indicates the output of the series-wound arrays is independent of the unit number. It is because the LST-TENG with high resistance connected in series in the circuit is equivalent to a disconnecting circuit, which is the most unsatisfying disadvantage for applying to the practical devices.

On the other hand, the output performance of the parallel arrays was also investigated and the results were shown in Fig. 5(d). It depicts a desirable growing output with the connected unit numbers, both the output voltage and current showed a linear rise with the unit amount.

The increase of the output voltage with the parallel unit number was also observed in the previous work[36]. The constant voltage of the parallel supply is based on the assumption that the internal resistance can be neglected, but the internal resistance of LST-TENG was too high to be ignored. Therefore, internal resistance is one of the most important parameters for the LST-TENGs. As can be seen in Fig. 5(d), the internal resistance of the LST-TENG arrays was reduced significantly with the parallel unit amount, which is the reason for the growing output voltage and current for the increasing parallel unit number. The peak current and peak load power of the LST-TENG array with 10 units with respect to various load resistance were measured to investigate the output performance and the results were displayed in Fig. 5(e). With the increase of load resistance, the peak current decreased and the output power first increased and then fall down. When the load resistance reached the internal resistance of the LST-TENG array obtained by the method mention above (obtained by Eq. (6)), the peak output power was 215 µW. The volumetric peak charge density and peak volumetric power density show optimal values of 0.73 mC/ m^3 and 228 mW/m^3, respectively. In the practical application, the improvement of the energy utilization efficiency is a crucial issue to make full use of LST-TENG with extra-high voltage, extra-low current and extremely high matching impedance[41]. It was demonstrated that the voltage output will change with the variable resistances of the sensor and the output power reached
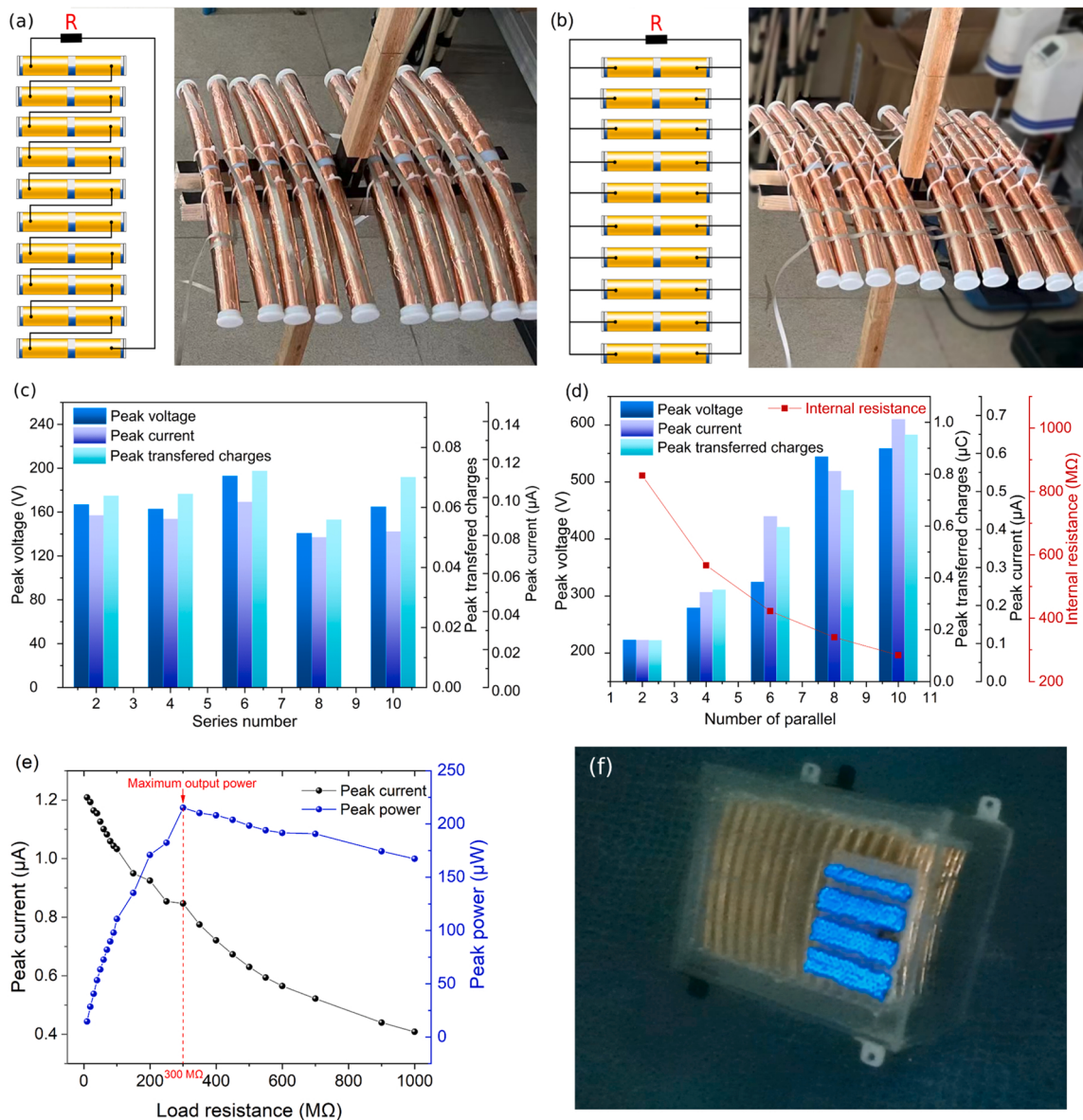
Fig. 5. Electrical characteristics of LST-TENG arrays. (a) Photograph and schematic diagram of the circuit for the series-wound LST-TENG array, (b) photograph and schematic diagram of the circuit of the parallel LST-TENG array, (c) relationship between the peak output and the unit number of the series-wound LST-TENG arrays, (d) variation of the peak output and internal resistance with the unit number of the parallel LST-TENG arrays, (e) peak current and peak output power of the parallel LST-TENG array with respect to the load resistance, (f) photograph of the LEDs lighted by the water wave driven LST-TENG block.

a high level when the external resistance is close to the internal resistance of TENG[42]. For self-powered devices, it is feasible to optimized the parallel number of the LST-TENG units to match he internal resistance with the external load resistance. To ensure the external load does not work at overcurrent conditions, the peak output should be determined by the external load, while the average/peak ratio affected by the electrodes could be set to adapt to the required output power.

Parallel connection is proved to be a feasible arrangement for the fabrication of the LST-TENG arrays, then the arrays were integrated within a sealed block and applied to harvest the water wave energy. Due to the high internal resistance, the output current for one TENG unit is low at 0.1 μA. The parallel TENG arrays where the internal resistance decreased and the output current increased with the unit number was used to match the electrical devices in the practical application. Moreover, the LST-TENG network is mainly used for the self-power offshore device required low current, such as beacon lights and sensors. As shown in Fig. 5(f), the LST-TENG block with 112 units running 520 LED lamps under the driving by the simulated water wave in the water tank. The

video that records the blink of the LEDs using alternating current is shown in the supplementary Video. S1.

Supplementary material related to this article can be found online at doi:10.1016/j.nanoen.2022.107810.

4. Conclusions

In conclusion, a liquid-solid tubular TENG was fabricated based on the contact electrification effect between PTFE and DI water. The influence of the TENG structure and motion characteristics on the electrical output performance were investigated to evaluate the electrical output quality of LST-TENG and explore the optimal approaches to integrated the LST-TENGs for the wave energy harvest. Diverse structural parameters regulate the LST-TENG unit in a synergistic or antagonistic manner, which provides a peak open-circuit voltage over 150 V and a peak short-circuit current over 0.1μA. To expand the application of the newly proposed LST-TENG, the electrical performance of the integrated LST-TENG units combined in series and parallel were compared to

provide guidance for the fabrication of the LST-TENG arrays to get high output. It was demonstrated the power density of the LST-TENG parallel arrays reached 228 mW/m^3 at the optimal condition. 112 LST-TENG units were packaged in parallel connection to achieve higher output, which was employed to harvest water wave energy to light up 520 LEDs. Considering the extremely high internal resistance of the LST-TENG unit, assembling a specific number of units into a TENG network to match the optimal output power condition can be used as a practical power supply for the self-power offshore devices. This paper is not only concerned with the improvement of the output performance, but the characteristics of the electrical output also investigated to provide the essential data for the matching of the integrated LST-TENG arrays and the self-power load.

CRediT authorship contribution statement

Qianxi Zhang: Methodology, Validation, Conceptualization, Investigation, Formal analysis. **Ming He:** Investigation, Writing – original draft, Visualization. **Xinxiang Pan:** Supervision, Project administration. **Dandan Huang:** Software, Validation. **Huahui Long:** Software, Validation. **Mingsheng Jia:** Methodology, Validation. **Zhiqiang Zhao:** Writing – review & editing, Visualization. **Cheng Zhang:** Methodology, Validation, Conceptualization. **Minyi Xu:** Supervision, Writing – review & editing. **Shishi Li**: Writing – original draft, Writing – review & editing.

Declaration of Competing Interest

The authors declare that they have no known competing financial interests or personal relationships that could have appeared to influence the work reported in this paper.

Data Availability

All data are available in the main text and the supplementary materials.

Acknowledgment

Appendix A. Supporting information

Supplementary data associated with this article can be found in the online version at doi:10.1016/j.nanoen.2022.107810.

References

[1] Y. Zou, J. Xu, J. Fang, X. Zhao, Y. Zhou, J. Chen, A hand-driven portable triboelectric nanogenerator using whirligig spinning dynamics, Nano Energy 83 (2021), 105845, https://doi.org/10.1016/j.nanoen.2021.105845.

[2] B. Zhang, F. Chun, G. Chen, T. Yang, A. Libanori, K. Chen, G. Conta, D. Xiong, C. Yan, W. Yang, J. Chen, Water-evaporation-induced intermolecular force for nano-wrinkled polymeric membrane, Cell Rep. Phys. Sci. 2 (6) (2021), 100441, https://doi.org/10.1016/j.xcrp.2021.100441.

[3] G. Chen, Y. Li, M. Bick, J. Chen, Smart textiles for electricity generation, Chem. Rev. 120 (8) (2020) 3668–3720, https://doi.org/10.1021/acs.chemrev.9b00821.

[4] T.W. Thorpe, A brief review of wave energy, UK Dep. Trade Ind. (1999). ETSU-R120.

[5] K. Gunn, C. Stock-Williams, Quantifying the global wave power resource, Renew. Energ. 44 (2012) 296–304, https://doi.org/10.1016/j.renene.2012.01.101.

[6] A. Clément, P. McCullen, A. Falcão, A. Fiorentino, F. Gardner, K. Hammarlund, G. Lemonis, T. Lewis, K. Nielsen, S. Petroncini, M.T. Pontes, P. Schild, B. Sjöström, H.C. Sørensen, T. Thorpe, Wave energy in Europe: current status and perspectives, Renew. Sust. Energ. Rev. 6 (5) (2002) 405–431, https://doi.org/10.1016/S1364-0321(02)00009-6.

[7] A. Samad, R. Suchithra, Marine power technology-wave energy. Sustainable Fuel Technologies Handbook, Acdemic Press, London, 2021, pp. 241–267.

[8] B. Ekergård, Full scale applications of permanent magnet electromagnetic energy converters: from Nd2Fe14B to ferrite. Uppsala University, Uppsala, 2013.

[9] L. Huang, M. Hu, J. Liu, H. Yu, C. Zeng, Z. Chen, Electromagnetic design of a 10-kW-Class Flux-Switching linear superconducting hybrid excitation generator for wave energy conversion, IEEE T. Appl. Supercon. 27 (4) (2017) 1–6, https://doi.org/10.1109/TASC.2017.2656620.

[10] P. Bai, G. Zhu, Z.H. Lin, Q. Jing, J. Chen, G. Zhang, J. Ma, Z.L. Wang, Integrated multilayered triboelectric nanogenerator for harvesting biomechanical energy from human motions, ACS Nano 7 (4) (2013) 3713–3719, https://doi.org/10.1021/nn4007708.

[11] H. Chen, Q. Lu, X. Cao, N. Wang, Z. Wang, Natural polymers based triboelectric nanogenerator for harvesting biomechanical energy and monitoring human motion, Nano Res. 15 (3) (2022) 2505–2511, https://doi.org/10.1007/s12274-021-3764-6.

[12] C. Wu, R. Liu, J. Wang, Y. Zi, L. Lin, Z.L. Wang, A spring-based resonance coupling for hugely enhancing the performance of triboelectric nanogenerators for harvesting low-frequency vibration energy, Nano Energy 32 (2017) 287–293, https://doi.org/10.1016/j.nanoen.2016.12.061.

[13] S. Liu, X. Li, Y. Wang, Y. Yang, L. Meng, T. Cheng, Z.L. Wang, Magnetic switch structured triboelectric nanogenerator for continuous and regular harvesting of wind energy, Nano Energy 83 (2021), 105851, https://doi.org/10.1016/j.nanoen.2021.105851.

[14] Y. Yao, T. Jiang, L. Zhang, X. Chen, Z. Gao, Z.L. Wang, Charging system optimization of triboelectric nanogenerator for water wave energy harvesting and storage, ACS Appl. Mater. Int. 8 (33) (2016) 21398–21406, https://doi.org/10.1021/acsami.6b07697.

[15] C. Rodrigues, M. Ramos, R. Esteves, J. Correia, D. Clemente, F. Gonçalves, N. Mathias, M. Gomes, J. Silva, C. Duarte, T. Morais, P. Rosa-Santos, F. Taveira-Pinto, A. Pereira, J. Ventura, Integrated study of triboelectric nanogenerator for ocean wave energy harvesting: performance assessment in realistic sea conditions, Nano Energy 84 (2021), 105890, https://doi.org/10.1016/j.nanoen.2021.105890.

[16] Y. Wang, X. Liu, Y. Wang, H. Wang, H. Wang, S.L. Zhang, T. Zhao, M. Xu, Z.L. Wang, Flexible seaweed-like triboelectric nanogenerator as a wave energy harvester powering marine internet of things, ACS Nano 15 (10) (2021) 15700–15709, https://doi.org/10.1021/acsnano.1c05127.

[17] X. Zhao, H. Askari, J. Chen, Nanogenerators for smart cities in the era of 5G and internet of things, Joule 5 (6) (2021) 1391–1431, https://doi.org/10.1016/j.joule.2021.03.013.

[18] J. Chen, J. Yang, Z. Li, X. Fan, Y. Zi, Q. Jing, H. Guo, Z. Wen, K.C. Pradel, S. Niu, Z.L. Wang, Networks of triboelectric nanogenerators for harvesting water wave energy: A potential approach toward blue energy, ACS Nano 9 (3) (2015) 3324–3331, https://doi.org/10.1021/acsnano.5b00534.

[19] G. Zhu, Y. Su, P. Bai, J. Chen, Q. Jing, W. Yang, Z.L. Wang, Harvesting water wave energy by asymmetric screening of electrostatic charges on a nanostructured hydrophobic thin-film surface, ACS Nano 8 (6) (2014) 6031–6037, https://doi.org/10.1021/nn5012732.

[20] Y. Xi, J. Wang, Y. Zi, X. Li, C. Han, X. Cao, C. Hu, Z. Wang, High efficient harvesting of underwater ultrasonic wave energy by triboelectric nanogenerator, Nano Energy 38 (2017) 101–108, https://doi.org/10.1016/j.nanoen.2017.04.053.

[21] L. Lin, Y. Xie, S. Niu, S. Wang, P.K. Yang, Z.L. Wang, Robust triboelectric nanogenerator based on rolling electrification and electrostatic induction at an instantaneous energy conversion efficiency of approximately 55%, ACS Nano 9 (1) (2015) 922–930, https://doi.org/10.1021/nn506673x.

[22] Y. Pang, S. Chen, Y. Chu, Z.L. Wang, C. Cao, Matryoshka-inspired hierarchically structured triboelectric nanogenerators for wave energy harvesting, Nano Energy 66 (2019), 104131, https://doi.org/10.1016/j.nanoen.2019.104131.

[23] L. Xu, T. Jiang, P. Lin, J.J. Shao, C. He, W. Zhong, X.Y. Chen, Z.L. Wang, Coupled triboelectric nanogenerator networks for efficient water wave energy harvesting, ACS Nano 12 (2) (2018) 1849–1858, https://doi.org/10.1021/acsnano.7b08674.

[24] P. Cheng, H. Guo, Z. Wen, C. Zhang, X. Yin, X. Li, D. Liu, W. Song, X. Sun, J. Wang, Z.L. Wang, Largely enhanced triboelectric nanogenerator for efficient harvesting of water wave energy by soft contacted structure, Nano Energy 57 (2019) 432–439, https://doi.org/10.1016/j.nanoen.2018.12.054.

[25] S. Jang, M. La, S. Cho, Y. Yun, J.H. Choi, Y. Ra, S.J. Park, D. Choi, Monocharged electret based liquid-solid interacting triboelectric nanogenerator for its boosted electrical output performance, Nano Energy 70 (2020), 104541, https://doi.org/10.1016/j.nanoen.2020.104541.

[26] D. Choi, D.W. Kim, D. Yoo, K.J. Cha, M. La, D.S. Kim, Spontaneous occurrence of liquid-solid contact electrification in nature: Toward a robust triboelectric nanogenerator inspired by the natural lotus leaf, Nano Energy 36 (2017) 250–259, https://doi.org/10.1016/j.nanoen.2017.04.026.

[27] H. Park, H.K. Kim, Y. Hwang, D. Shin, Water-through triboelectric nanogenerator based on Ti-mesh for harvesting liquid flow, J. Korean Phys. Soc. 72 (4) (2018) 499–503, https://doi.org/10.3938/jkps.72.499.

[28] X.J. Zhao, S.Y. Kuang, Z.L. Wang, G. Zhu, Highly adaptive Solid-Liquid interfacing triboelectric nanogenerator for harvesting diverse water wave energy, ACS Nano 12 (5) (2018) 4280–4285, https://doi.org/10.1021/acsnano.7b08716.

[29] L. Liu, Q. Shi, J.S. Ho, C. Lee, Study of thin film blue energy harvester based on triboelectric nanogenerator and seashore IoT applications, Nano Energy 66 (2019), 104167, https://doi.org/10.1016/j.nanoen.2019.104167.

[30] Y. Wang, Z. Wang, D. Zhao, X. Yu, T. Cheng, G. Bao, Z.L. Wang, Flow and level sensing by waveform coupled liquid-solid contact-electrification, Mater. Today Phys. 18 (2021), 100372, https://doi.org/10.1016/j.mtphys.2021.100372.

[31] X. Zhang, Y. Zheng, D. Wang, Z.U. Rahman, F. Zhou, Liquid-solid contact triboelectrification and its use in self-powered nanosensor for detecting organics in

water, Nano Energy 30 (2016) 321–329, https://doi.org/10.1016/j.nanoen.2016.10.025.

[32] B. Wang, Y. Wu, Y. Liu, Y. Zheng, Y. Liu, C. Xu, X. Kong, Y. Feng, X. Zhang, D. Wang, New hydrophobic organic coating based triboelectric nanogenerator for efficient and stable hydropower harvesting, ACS Appl. Mater. Inter. 12 (28) (2020) 31351–31359, https://doi.org/10.1021/acsami.0c03843.

[33] W. Sun, Y. Zheng, T. Li, M. Feng, S. Cui, Y. Liu, S. Chen, D. Wang, Liquid-solid triboelectric nanogenerators array and its applications for wave energy harvesting and self-powered cathodic protection, Energy (Oxf.) 217 (2021), 119388, https://doi.org/10.1016/j.energy.2020.119388.

[34] W. Xu, J. Yang, S. Liu, Y. Meng, D. Feng, L. Jia, S. Liu, B. Wang, X. Li, An instantaneous discharging liquid-solid triboelectric nanogenerator (IDLS-TENG) with boosted peak power output, Nano Energy 86 (2021), 106093, https://doi.org/10.1016/j.nanoen.2021.106093.

[35] L. Zhang, X. Li, Y. Zhang, Y. Feng, F. Zhou, D. Wang, Regulation and influence factors of triboelectricity at the solid-liquid interface, Nano Energy 78 (2020), 105370, https://doi.org/10.1016/j.nanoen.2020.105370.

[36] H. Wu, Z. Wang, Y. Zi, Multi-mode water-tube-based triboelectric nanogenerator designed for low-frequency energy harvesting with ultrahigh volumetric charge density, Adv. Energy Mater. 11 (16) (2021) 2100038, https://doi.org/10.1002/aenm.202100038.

[37] J. Oh, J. Kim, J. Lee, H. Park, T. Komatsu, Design and analysis of wave energy converter for a buoy, J. Mech. Sci. Technol. 21 (12) (2007) 2005–2010, https://doi.org/10.1007/BF03177458.

[38] X. Chen, L. Gao, J. Chen, S. Lu, H. Zhou, T. Wang, A. Wang, Z. Zhang, S. Guo, X. Mu, Z.L. Wang, Y. Yang, A chaotic pendulum triboelectric-electromagnetic hybridized nanogenerator for wave energy scavenging and self-powered wireless sensing system, Nano Energy 69 (2020), 104440, https://doi.org/10.1016/j.nanoen.2019.104440.

[39] J. Nie, Z. Ren, L. Xu, S. Lin, F. Zhan, X. Chen, Z.L. Wang, Probing contact-electrification-induced electron and ion transfers at a liquid-solid interface, Adv. Mater. (Weinh.) 32 (2) (2020), e1905696, https://doi.org/10.1002/adma.201905696.

[40] S. Lin, L. Xu, A. Chi Wang, Z.L. Wang, Quantifying electron-transfer in liquid-solid contact electrification and the formation of electric double-layer, Nat. Commun. 11 (1) (2020) 399, https://doi.org/10.1038/s41467-019-14278-9.

[41] X. Cheng, L. Miao, Y. Song, Z. Su, H. Chen, X. Chen, J. Zhang, H. Zhang, High efficiency power management and charge boosting strategy for a triboelectric nanogenerator, Nano Energy 38 (2017) 438–446, https://doi.org/10.1016/j.nanoen.2017.05.063.

[42] Q. Shen, X. Xie, M. Peng, N. Sun, H. Shao, H. Zheng, Z. Wen, A.X. Sun, Self-Powered vehicle emission testing system based on coupling of triboelectric and chemoresistive effects, Adv. Funct. Mater. 28 (2018) 1703420, https://doi.org/10.1002/adfm.201703420.

Xinxiang Pan received his B.E and Ph.D. degrees from Marine Engineering College, Dalian Maritime University, China, in 1987 and 1999. He now is President of Guangdong Ocean University. His research interests include smart and green ship, ocean engineering, energy saving and emission reduction, ship safety and pollution control, microfluidic chip, nano energy and self-powered systems.

Dandan Huang is currently pursuing her postgraduate degree in Guangdong Ocean University of China. Her research is focused on liquid-solid triboelectric nanogenerators to harvest blue energy.

Huahui Long, a postgraduate student, is currently studying for his master's degree in Guangdong Ocean University. His current research interest is in triboelectric nanogenerators.

Dr. Qianxi Zhang received his Ph.D. degree from Sun Yat-sen University in 2018. Now he is an associate professor in the School of Mechanical and Power Engineering, Guangdong Ocean University. His current research is mainly focused on the areas of triboelectric nano-generators, self-powered systems and blue energy.

Prof. Mingsheng Jia received his master's degree from Sichuan University, China in 1989. Now he is a professor in the School of Mechanical and Power Engineering, Guangdong Ocean University. His research is mainly focused on clean combustion and pollution control, heat transfer and energy-saving equipment, new energy technology.

Ming He is currently studying for a master's degree in Guangdong Ocean University of China. His current research interests include blue energy collection, self-powered systems, and liquid-solid triboelectric nanogenerators.

Lectr. Zhiqiang Zhao received his Master degree in Marine Engineering College from Dalian Maritime University in 2015. Now he is a lecturer in Guangdong Ocean University. His current research is mainly focused on the triboelectric nano-generators in green energy development and sensor technology.

Dr. Cheng Zhang received his Ph.D. degree in Thermal Engineering from Huazhong University of Science and Technology in 2018. Now he is a faculty of School of Ocean and Energy, Guangdong Ocean University. His current research is mainly focused on solar energy and triboelectric nanogenerators.

Dr. Shishi Li received her Ph.D. degree from South China University of Technology in 2021. Now she is a lecturer in Guangdong Ocean University. Her current research is mainly focus on the efficient conversion and clean utilization of energy.

Dr. Minyi Xu received his Ph.D. degree from Peking University in 2012. During 2016–2017, he joined Professor Zhong Lin Wang' group at Georgia Institute of Technology. Now he is a Professor in the Marine Engineering College, Dalian Maritime University. His current research is mainly focused on the areas of blue energy, self-powered systems, triboelectric nano-generators and its practical applications in smart ship and ocean.